On the 2018 Outburst of the Accreting Millisecond X-Ray Pulsar Swift J1756.9–2508 As Seen with NICER

Peter Bult[1], Diego Altamirano[2], Zaven Arzoumanian[1], Deepto Chakrabarty[3], Keith C. Gendreau[1], Sebastien Guillot[4,5], Wynn C. G. Ho[6,7], Gaurava K. Jaisawal[8], Steven Lentine[9], Craig B. Markwardt[1], Son N. Ngo[10], John S. Pope[11], Paul S. Ray[12], Maxine R. Saylor[11], and Tod E. Strohmayer[13]

[1] Astrophysics Science Division, NASA's Goddard Space Flight Center, Greenbelt, MD 20771, USA
[2] Physics and Astronomy, University of Southampton, Southampton, Hampshire SO17 1BJ, UK
[3] MIT Kavli Institute for Astrophysics and Space Research, Massachusetts Institute of Technology, Cambridge, MA 02139, USA
[4] CNRS, IRAP, 9 avenue du Colonel Roche, BP 44346, F-31028 Toulouse Cedex 4, France
[5] Université de Toulouse, CNES, UPS-OMP, F-31028 Toulouse, France
[6] Department of Physics and Astronomy, Haverford College, 370 Lancaster Avenue, Haverford, PA 19041, USA
[7] Mathematical Sciences, Physics and Astronomy, and STAG Research Centre, University of Southampton, Southampton SO17 1BJ, UK
[8] National Space Institute, Technical University of Denmark, Elektrovej 327-328, DK-2800 Lyngby, Denmark
[9] Chesapeake Aerospace and Instrument Projects Division, NASA's Goddard Space Flight Center, Greenbelt, MD 20771, USA
[10] Mechanical Systems Division, NASA's Goddard Space Flight Center, Greenbelt, MD 20771, USA
[11] KBRWyle and Software Engineering Division, NASA's Goddard Space Flight Center, Greenbelt, MD 20771, USA
[12] Space Science Division, Naval Research Laboratory, Washington, DC 20375-5352, USA
[13] Astrophysics Science Division and Joint Space-Science Institute, NASA's Goddard Space Flight Center, Greenbelt, MD 20771, USA

Abstract

We report on the coherent timing analysis of the 182 Hz accreting millisecond X-ray pulsar Swift J1756.9−2508 during its 2018 outburst as observed with the Neutron Star Interior Composition Explorer (NICER). Combining our NICER observations with *Rossi X-ray Timing Explorer* observations of the 2007 and 2009 outbursts, we also studied the long-term spin and orbital evolution of this source. We find that the binary system is well described by a constant orbital period model, with an upper limit on the orbital period derivative of $|\dot{P}_b| < 7.4 \times 10^{-13}$ s s^{-1}. Additionally, we improve upon the source coordinates through astrometric analysis of the pulse arrival times, finding R.A. $= 17^h56^m57\overset{s}{.}18 \pm 0\overset{s}{.}08$ and decl. $= -25°06'27\overset{''}{.}8 \pm 3\overset{''}{.}5$, while simultaneously measuring the long-term spin frequency derivative as $\dot{\nu} = -7.3 \times 10^{-16}$ Hz s^{-1}. We briefly discuss the implications of these measurements in the context of the wider population of accreting millisecond pulsars.

Key words: stars: neutron – X-rays: binaries – X-rays: individual (Swift J1756.9–2508)

1. Introduction

Accreting millisecond X-ray pulsars (AMXPs; Wijnands & van der Klis 1998) are rapidly rotating neutron stars whose spin periods can be observed directly as coherent oscillations in their X-ray light curves. By monitoring the frequency evolution of such pulsations on years-long timescales, we can measure the rate of spin change and gain insight into intrinsic properties of the neutron star. Additionally, precise timing measurements enable detailed studies of the binary orbit, offering potential insight into the binary evolution of millisecond pulsars. Such long-term monitoring efforts, however, are complicated by the transient nature of these AMXPs. The pulsar is visible only during X-ray outbursts, when the source is actively accreting. Such outbursts typically last for a number of days to weeks, and may be interspersed by years or even decades of quiescence.

Of the population of AMXPs currently known (Patruno & Watts 2012; Sanna et al. 2017b, 2018; Strohmayer & Keek 2017), only eight sources have shown recurrent outbursts, and of those only three could be studied with sufficient precision to allow for the long-term spin frequency derivative to be measured. Studies considering the binary orbit of AMXPs face a similar situation: a physically interesting sensitivity to the orbital period rate of change has been achieved for only three AMXPs. One of these seems consistent with a slow evolution driven by angular momentum loss through gravitational radiation (Patruno 2017; Sanna et al. 2017c), the other

two evolve on a markedly faster timescale (Patruno et al. 2012; Sanna et al. 2017a, although see also Patruno et al. 2017 for a detailed discussion of these and other classes of binary systems). It is therefore of considerable interest to increase the sample size of this population.

The AMXP Swift J1756.4−2508 (hereafter Swift J1756) was first discovered in 2007 June (Krimm et al. 2007a) and was quickly found to be a 182 Hz pulsar (Markwardt et al. 2007). It was observed in outburst again in 2009 July (Patruno et al. 2009), but remained in quiescence for the following 9 years. The *Rossi X-ray Timing Explorer* (*RXTE*) observed both outbursts extensively; nonetheless, a detailed analysis of those data (Patruno et al. 2010) did not detect a spin frequency change: with only two reported outbursts, both of short duration, the upper limit on the spin frequency derivative was $|\dot{\nu}| < 3 \times 10^{-13}$ Hz s^{-1}, which is much larger than any neutron star spin-down observed in similar sources.

On 2018 April 3 *INTEGRAL* reported a new outburst from Swift J1756 (Mereminskiy et al. 2018). Follow-up observations with the Neutron Star Interior Composition Explorer (NICER; Gendreau & Arzoumanian 2017) quickly revealed the presence of 182 Hz pulsations (Bult et al. 2018a), confirming the third known outburst of this AMXP. With an observational baseline that spans over a decade, we may now probe a physically interesting regime of spin-down parameters. In this work, we present a coherent timing analysis of the NICER campaign for the recent Swift J1756

outburst, together with archival data for the earlier outburst episodes.

2. Observations

The NICER X-ray Timing Instrument consists of an array of 56 concentrator X-ray optics paired with silicon drift detectors (Gendreau et al. 2016). These detectors are sensitive in the 0.2–12 keV energy band (Prigozhin et al. 2012), with an energy resolution of better than 150 eV, and a timing precision of ~100 ns rms. We observed Swift J1756 with 52 operating detectors, giving a total effective area of ~1900 cm^2 at 1.5 keV.

We monitored Swift J1756 from 2018 April 4 until 2018 April 25, at which time the source had returned to quiescence (Bult et al. 2018b). For this paper, we analyzed all available NICER data (ObsID 1050230101 through 1050230108), which together amounted to 54 ks of unfiltered exposure.

We processed the data using HEASOFT version 6.24 and NICERDAS version 2018-04-06_V004. The data were cleaned using standard filtering criteria: we selected only those epochs that had a pointing offset $<54''$, bright Earth limb angle $>40°$, dark Earth limb angle $>30°$, and were outside the South Atlantic Anomaly (SAA). After processing we were left with 42 ks of exposure.

Next we computed the 12–15 keV light curve using 8 s bins. Above 12 keV the performance of the detectors and X-ray optics has diminished such that essentially no astrophysical signal is expected. Nonetheless, we observed several epochs during which the count rate in this light curve was greater than 1 ct/s, which we attributed to periods of increased background. Since these intervals were correlated with an elevated count rate in the 0.4–10 keV light curve, we removed them from the analysis. An additional 1 ks of exposure was removed in this way.

Finally, we were left with 41 ks of good time exposure. We applied barycentric corrections to those events using the FTOOL BARYCORR with the source coordinates of Krimm et al. (2007b) and the DE405 Solar System ephemeris. No X-ray bursts were observed.

Because NICER does not have imaging capabilities, we used NICER observations of the *RXTE* blank field region 8 (Jahoda et al. 2006) to estimate the background count rate. Applying the same filtering criteria, we obtained 74 ks of good background field exposure, yielding an averaged background rate of 2 ct/s in the 0.4–10 keV band.

3. Analysis and Results

For the coherent timing analysis, we selected all events in the 0.4–10 keV energy range and corrected the photon arrival times for the source binary motion using the ephemeris reported by Patruno et al. (2010). Assuming a constant orbital period, we could extrapolate the orbital phase to the current epoch, yielding a predicted time of passage through the ascending node, T_{asc}, in terms of MJD(TDB) of

$$T_{asc,pred} = 58211.0170 \pm 0.0002.$$

As the 1σ uncertainty on this extrapolation is only about 0.5% of the orbital period, the orbital solution allowed for a coherent propagation across the nine years of quiescence since the last outburst. To test this prediction, we searched a grid of T_{asc} values in steps of 1×10^{-5} days spanning one full orbit and

Table 1
Timing Solution for the 2018 Outburst of Swift J1756

Parameter	Value	Uncertainty
ν (Hz)	182.0658037800	4.5×10^{-8}
$a_x \sin i$ (lt-ms)	5.981	4.6×10^{-2}
P_b (s)	3282.463	9.5×10^{-2}
T_{asc} (MJD)	58211.017496	8.4×10^{-5}
ϵ	$<1 \times 10^{-2}$	⋯
χ^2/dof	16.6/16	⋯

Note. Uncertainties give the 1σ statistical errors and the upper limit is quoted at the 95% c.l. The ϵ parameter gives the orbital eccentricity.

folded the data on each trial ephemeris. The highest pulse amplitude was found at $T_{asc,grid} = 58211.01736$, which is consistent with the extrapolated solution. We adopted the results from our grid search as our initial trial ephemeris.

Next, we divided the data into segments of ~1000 s exposure. For each segment, we used the trial ephemeris to remove the orbital modulation and then folded on the pulse period. The resulting pulse profiles were fit with a constant plus two sinusoids, where one sinusoid was set at the spin frequency and the second at twice that frequency, so to capture the fundamental and second harmonic, respectively. A pulse harmonic was considered to be significant when its amplitude divided by its statistical uncertainty was greater than three, that is, when $A/\sigma_A > 3$. Under this condition a third harmonic was never required. Pulse amplitudes are reported in terms of fractional rms

$$r_i = \frac{1}{\sqrt{2}} \frac{A_i}{N_\gamma - B}, \tag{1}$$

where A_i is the measured sinusoidal amplitude of the ith harmonic, N_γ is the total number of photons in the considered segment, and B is the estimated number of background events in that segment. We further note that rms amplitudes are smaller than sinusoidal amplitudes by a factor of $\sqrt{2}$.

As the pulse profiles of AMXPs may change over time (see, e.g., Patruno & Watts 2012, for a review), we modeled the measured pulse arrival times for each harmonic separately. For both harmonics, we adopted a timing model consisting of a circular orbit and constant spin frequency. Hence, our model consisted of four parameters: the binary orbital period P_b, the projected semimajor axis $a_x \sin i$, the time of ascending node T_{asc}, and the spin frequency ν. We fit this model to the data using TEMPO2 (Hobbs et al. 2006) and iterated the procedure of folding and refitting until the timing solution had converged.

The phases of the fundamental pulsation are well described by the timing model, with goodness-of-fit statistic of $\chi^2 = 16.6$ for 16 degrees of freedom (dof, see Table 1). The second harmonic, on the other hand, shows significant residual deviations ($\chi^2 = 25.7$, 7 dof). These residuals can be attributed to timing noise, which was also present in the second harmonic of the previous outbursts (Patruno et al. 2010).

The pulse evolution for our best-fit timing solution is shown in Figure 1. The top panel gives the count rate in each segment, and shows how the source count rate decayed steadily from April 3 (MJD 58211) to April 12 (MJD 58220). The additional observation on April 25 (MJD 58233) is not shown, as the source was in quiescence. The middle panel gives the fractional
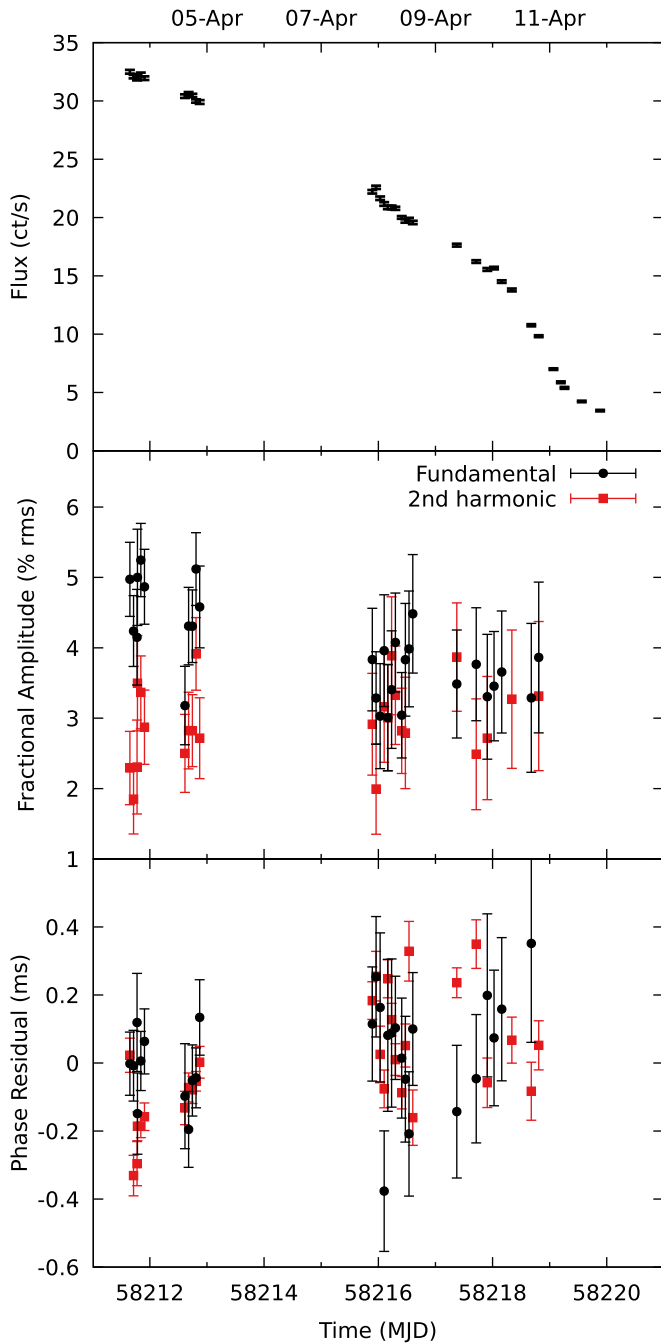
Figure 1. Outburst and pulse evolution of Swift J1756 for ~1 ks segments. Top: 0.4–10 keV light curve (source+background). Middle: fractional amplitudes of the fundamental pulsation (black) and second harmonic (red). Bottom: phase residuals of the pulsations with respect to the ephemeris reported in Table 1. Upper limits on nondetections of individual harmonics are not shown.

Figure 2. Energy dependent properties for the fundamental (black) and second harmonic (red) of the pulsations, with (top) pulse fractional amplitude and (bottom) pulse time-lags with respect to the timing model reported in Table 1.

amplitudes of the fundamental pulsation and second harmonic. Finally, the bottom panel gives the residual phase variations. These residuals show that the data are well described by a circular orbit model, and no anomalous phase jumps are observed. The orbital parameters of our best-fit solution are shown in Table 1.

We also considered the energy dependence of the pulsations. We divided the 0.4–10 keV energy range into seven bins, each about 1 keV wide. For each bin, we then applied the timing solution reported in Table 1 and folded all data into a single
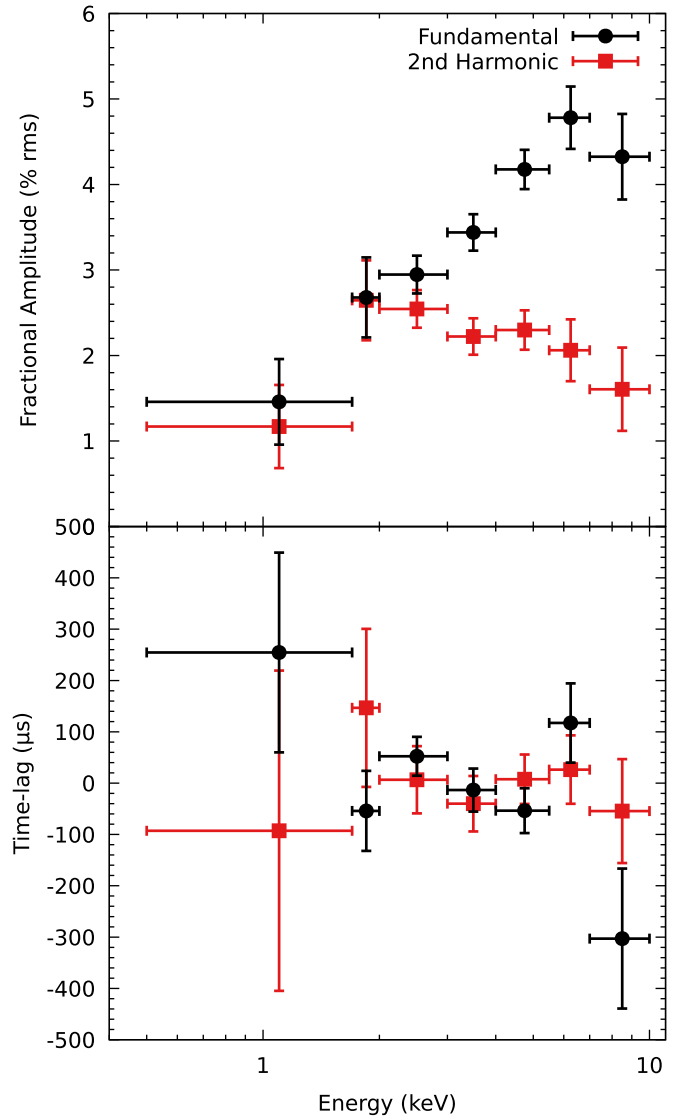
pulse profile. We measured the amplitudes of the fundamental and second harmonic, as well as their relative phases. As shown in Figure 2 (top panel), the fractional amplitude of the fundamental increases with energy, while the second harmonic shows a slight decline in its fractional amplitude. For both harmonics the phase residuals are approximately constant across the NICER passband (Figure 2, bottom panel).

3.1. Orbital Evolution

The orbital period measured for the 2018 outburst of Swift J1756 is consistent with the orbital period reported by Patruno et al. (2010) within their combined 1σ statistical uncertainty. To obtain a more accurate measure of the orbital evolution, we performed a coherent analysis of the orbital phase across all three outbursts.

Following the procedure outlined in Hartman et al. (2008), we compared the predicted evolution of the best known orbital ephemeris with the orbital phases measured in each of the three outbursts. Specifically, we calculate the residual time of
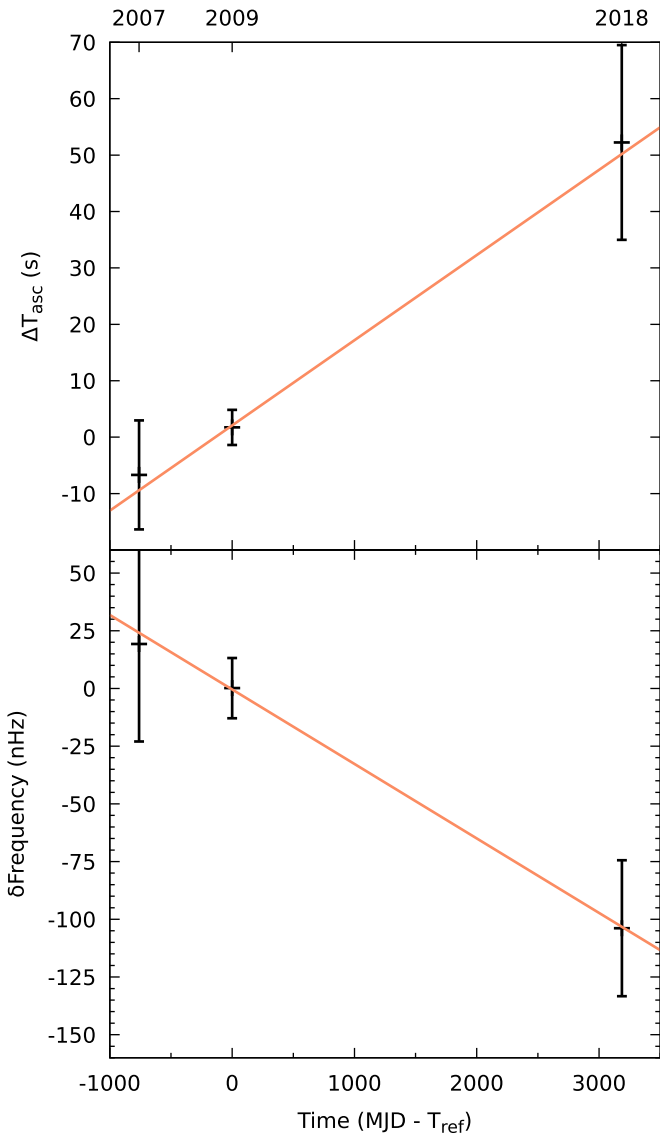
Figure 3. Long-term evolution of Swift J1756, showing (top) evolution of the time of ascending node with respect to the ephemeris of Patruno et al. (2010) and (bottom) pulse frequencies relative to offset frequency $\nu_0 = 182.065803903$ Hz for each of the three outbursts. The reference time is $T_{\rm ref} = 55026.03429$. Solid lines show best-fit models (see the text for details).

passage through the ascending node, $\Delta T_{\rm asc}$, as

$$\Delta T_{\rm asc} = T_{{\rm asc},i} - (T_{\rm ref} + NP_b), \qquad (2)$$

where $T_{{\rm asc},i}$ is the time of ascending node for the ith outburst, N is the integer number of orbital cycles between the ith outburst and the reference time, and we used the reference time, $T_{\rm ref}$, and orbital period, P_b, as reported in Table 4 of Patruno et al. (2010).

As shown in Figure 3 (top panel), we found that the residual $T_{\rm asc}$ shows a steady advance over time, indicating that the orbital period, $P_{b,{\rm trial}}$, used to obtain these values underestimates the actual period. Indeed, these residuals are poorly described by a constant ($\chi^2 = 9.3$, 2 dof), and instead prefer a linear model as

$$\Delta T_{\rm asc} = N\delta P_b, \qquad (3)$$

with a best-fit statistic of $\chi^2 = 0.6$ for 2 degrees of freedom. This fit gives us a correction to (improvement of)

Table 2
Best-fit Timing Parameters of Swift J1756 from the
Joint Analysis of the 2007–2018 Outbursts

Parameter	Value	Uncertainty
R.A. (J2000)	$17^{\rm h}56^{\rm m}57\!\!\overset{\rm s}{.}18$	$0\!\!\overset{\rm s}{.}08$
Decl.(J2000)	$-25°06'27\!\!\overset{''}{.}8$	$3\!\!\overset{''}{.}5$
ν_0 (Hz)	182.065804074	8.3×10^{-8}
$\dot\nu$ (Hz s^{-1})	-7.3×10^{-16}	2.6×10^{-16}
P_b (s)	3282.352018	4.7×10^{-5}
$|\dot P_b|$ (s s^{-1})	$<7.4 \times 10^{-13}$	
$a_x \sin i$ (lt-ms)	5.965	1.3×10^{-2}
$T_{\rm asc}$ (MJD)	55026.034350	1.4×10^{-5}
ϵ	$<1 \times 10^{-2}$	...
$\chi^2/{\rm dof}$	218.5/196	...

Note. The spin frequency reference epoch is set at MJD 55026.6. Uncertainties give the 1σ statistical error and upper limits are quoted at the 95% c.l., with ϵ giving the binary eccentricity. Declination was not included in the fit.

the constant orbital period of $\delta P_b = 5.8 \times 10^{-4}$ s, such that $P_b = P_{b,{\rm trial}} + \delta P_b$; however, the very low χ^2 suggests that the uncertainties obtained from this fit may not be reliable.

For a more robust estimate of the long-term orbital evolution, we instead analyze all three outbursts simultaneously. We first reconstructed the pulse arrival times of the 2007 and 2009 outbursts, by repeating the analysis procedures described in Patruno et al. (2010). We then fit our timing model to all three outbursts at once. In this fit, the orbital parameters were coupled and the spin frequency was left free for each of the three outbursts (see, e.g., Bult et al. 2015). This procedure gives a good fit to the data ($\chi^2 = 226.2$, 197 dof), and yields an orbital period correction of $\delta P_b = (5.2 \pm 0.5) \times 10^{-4}$ s, which is consistent with the previously mentioned linear fit. The complete set of best-fit orbital parameters is reported in Table 2.

An orbital period derivative was not required to obtain a good fit to outbursts of Swift J1756, hence we found no evidence that the orbital period changed over the observed time span of 11 years. By adding this parameter to the joint-fit procedure, we obtained a 95% confidence level upper limit on the orbital period derivative of $|\dot P_b| < 7.4 \times 10^{-13}$ s s^{-1}.

3.2. Spin Frequency Evolution

The joint analysis described in the previous section gave us a local spin frequency measurement for each of the three outbursts. The measured frequencies for the 2007 and 2009 outbursts (Figure 3; bottom panel) were consistent with those reported by Patruno et al. (2010) within their 1σ statistical uncertainties. Combined with the spin frequency measured for the 2018 outburst as observed with NICER, we found a clear decline in spin frequency over time. Indeed, a constant spin frequency model gave a poor description of these data ($\chi^2 = 11.1$, 2 dof), whereas a linear model of the form

$$\Delta\nu = \delta\nu + \dot\nu T \qquad (4)$$

did better ($\chi^2 = 0.02$ for 1 degrees of freedom). The spin frequency derivative implied by this fit is on the order of -4×10^{-16} Hz s^{-1}. These measurements, however, are subject to a systematic bias associated with the uncertainty of the source coordinates (Manchester & Peters 1972). The best
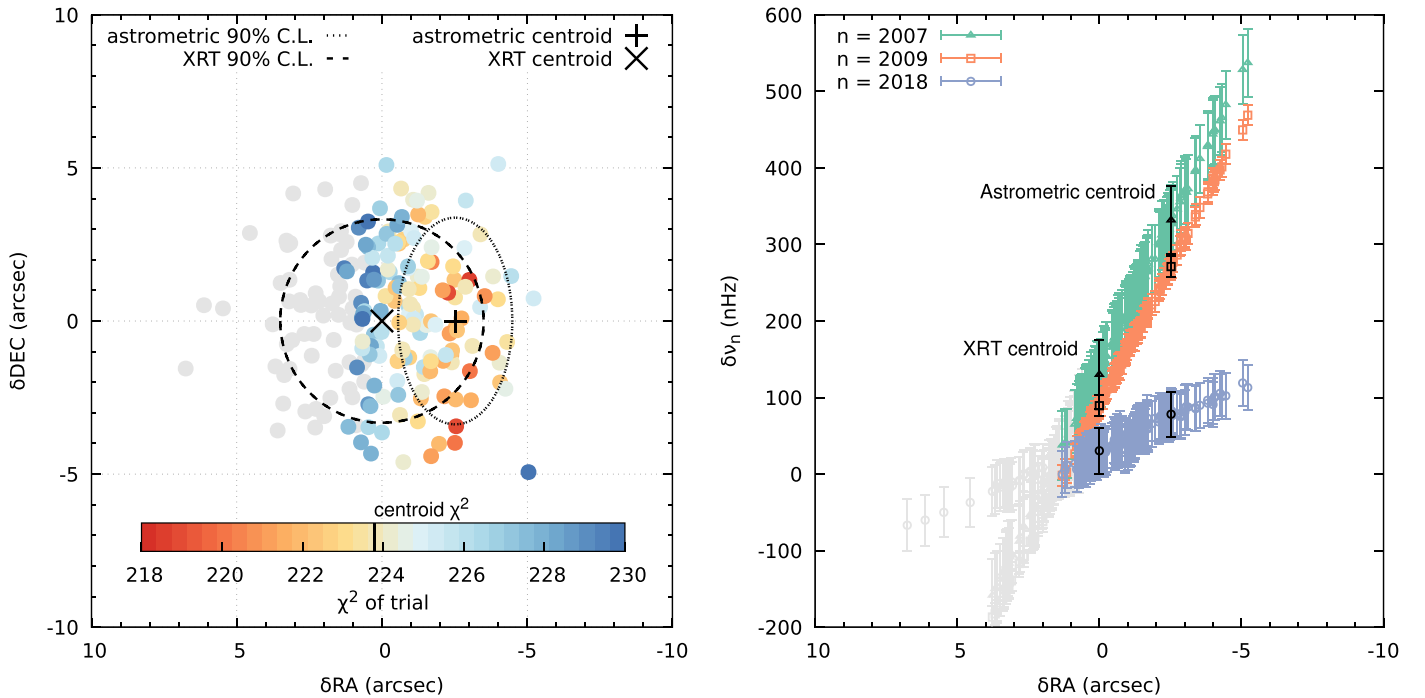
Figure 4. Results from a Monte Carlo (MC) study of the influence of the source position uncertainty on the performance of the timing model. Left: the MC trials relative to the centroid of the *Swift*/XRT source position (Krimm et al. 2007b), with the color coding indicating the χ^2 of the best-fit timing model for those coordinates. Also shown are the *Swift*/XRT centroid position and the astrometric position derived in this work, along with their respective 90% c.l. contours. Right: the spin frequency measured per outburst for the MC trials. Spin frequencies are shown relative to ν_0 (see Figure 3). The black points mark the spin frequencies retrieved at the astrometric and *Swift*/XRT centroid positions, as indicated. In both panels, points in gray represent MC trials that were rejected by the timing model fit (see Section 3.2 for details).

available source coordinates were obtained with *Swift*/XRT (Krimm et al. 2007b) and have a comparatively large uncertainty of $3\overset{''}{.}5$ (90% c.l.). A first-order estimate of the effect that this uncertainty has on the spin frequency derivative (Burderi et al. 2007; Hartman et al. 2008) gives $\sigma_{\dot{\nu},\mathrm{pos}} \sim 10^{-15}$ Hz s^{-1}, which is comparable to the slope observed in Figure 3. Hence, a more careful analysis is required.

To assess the effects of the source position uncertainty on our timing analysis, we generated 500 random coordinates distributed according to the *Swift*/XRT error circle. For each trial position, we reapplied the barycentric corrections and fit the timing model to the three outbursts jointly. We then measured, as a function of δRA and δDEC relative to the *Swift*/XRT centroid, the χ^2 of the timing model fit (which has 196 dof), and the spin frequency in each of the three outbursts. The results of these fits are summarized in Figure 4.

Shown in the left panel are the χ^2 values of the timing model fit, with the colored points indicating the trials for which this fit was statistically acceptable (*p*-value better than 0.05). Clearly the timing model is sensitive to δRA, implying that we can refine the source position. The timing model cannot constrain δDEC; however, given that Swift J1756 is located only $1\overset{\circ}{.}67$ away from the ecliptic, this is not surprising. As shown in the right panel of Figure 4, we additionally found that the spin frequencies measured per outburst tend to diverge for decreasing δRA, which is the region of parameter space that is clearly favored by the timing solution. To capture both effects, we searched for the minimum of the χ^2 space as a function of δRA[14] and scanned the χ^2 space out to $\Delta\chi^2 = 1$ to

---

[14] Note that this is equivalent to including R.A. as a free parameter in the timing model.

determine the position uncertainty. This gave a best-fit position of δRA $= -2\overset{''}{.}5 \pm 1\overset{''}{.}1$. We then measured the spin frequency derivative at the contours of our scan in δRA to determine the range of allowed values. Adding also (in quadrature) the statistical uncertainty of the linear fit to the long-term spin frequency trend, we then arrive at a spin frequency derivative measurement of $\dot{\nu} = (-7.3 \pm 2.6) \times 10^{-16}$ Hz s^{-1} (see Table 2 for the complete best-fit timing solution, including the refined source position).

4. Discussion

We reported on the coherent timing analysis of the 2018 outburst of Swift J1756 as observed with NICER. Consistent with analyses of the previous outbursts (Krimm et al. 2007b; Patruno et al. 2010), we find that the X-ray pulsations have energy dependent amplitudes; the fractional amplitude of the fundamental increases with energy, whereas the fractional amplitude of the harmonic shows a slight decline with energy. This energy dependent behavior is not unusual in AMXPs (Patruno & Watts 2012) and can be interpreted in terms of the thermal emission from the stellar hotspot and reprocessing in the accretion column (e.g., Gierliński et al. 2002; Ibragimov & Poutanen 2009).

The pulse arrival times of the 2018 outburst are well described by a timing model consisting of a circular orbit with a constant spin frequency. The pulse phases with respect to this model do not show spurious residuals with time or orbital phase, and no evidence is found that the pulse arrival times exhibit an additional delay associated with passing through the gravitational well of the companion star (Shapiro delay). We note, however, that the expected Shapiro delay is given as

(Shapiro et al. 1971)

$$\Delta t_S(\Phi) = -2\frac{GM_C}{c^3}(1 - \sin i \sin \Phi), \qquad (5)$$

where Φ is the orbital phase, G is the gravitational constant, c is the speed of light, and i is the inclination. Even for the maximum allowed companion mass, $M_C = 0.030\,M_\odot$ (Krimm et al. 2007b, but see Section 4.2 for more details) and an inclination of $90°$, the largest delay we can expect is only $4\,\mu s$. As this time-delay is smaller than the uncertainty on our phase residuals by nearly two orders of magnitude (see Figure 1), we are not sensitive to Shapiro delays in Swift J1756.

Comparing our measurements for the 2018 outburst with those of the 2007 and 2009 outbursts as observed with *RXTE*, we analyzed the long-term evolution of this source. We found that the binary system is consistent with having a constant orbital period and that the pulsar shows a spin frequency derivative of $\dot{\nu} = -7.3 \times 10^{-16}\,\mathrm{Hz\,s^{-1}}$.

4.1. Spin-down Evolution

The long-term spin frequency derivative measured in Swift J1756 is of the same order as the spin frequency derivatives measured in other AMXPs (Hartman et al. 2008; Patruno 2010; Riggio et al. 2011). This frequency change is most likely driven by the neutron star's loss of rotational energy. If so, then the spin-down luminosity is given as

$$\dot{E}_{sd} = 5 \times 10^{33}\left(\frac{I}{10^{45}\,\mathrm{g\,cm^2}}\right)\left(\frac{\nu}{182\,\mathrm{Hz}}\right)$$
$$\times \left(\frac{-\dot{\nu}}{7.3 \times 10^{-16}\,\mathrm{Hz\,s^{-1}}}\right)\mathrm{erg\,s^{-1}}, \qquad (6)$$

where I represents the neutron star moment of inertia.

The long-term spin-down of a neutron star is usually assumed to be dominated by the braking torque associated with a spinning magnetic field. Assuming this mechanism is responsible for the observed spin-down in Swift J1756, we can compute the magnetic dipole moment as (Spitkovsky 2006)

$$\mu = 2.9 \times 10^{26}\,(1 + \sin^2\alpha)^{-1/2}$$
$$\times \left(\frac{I}{10^{45}\,\mathrm{g\,cm^2}}\right)^{1/2}\left(\frac{\nu}{182\,\mathrm{Hz}}\right)^{-3/2}$$
$$\times \left(\frac{-\dot{\nu}}{7.3 \times 10^{-16}}\right)^{1/2}\mathrm{G\,cm^3}, \qquad (7)$$

where α is the misalignment angle between the rotational and magnetic poles. Considering $\alpha = 0°–90°$, we then find a magnetic field strength of $B \simeq (4–6) \times 10^8\,\mathrm{G}$ at the stellar magnetic poles. This magnetic field strength estimate is in line with those obtained for other accreting millisecond pulsars (see Mukherjee et al. 2015 and references therein).

4.2. Orbit Evolution

The observed long-term binary evolution of Swift J1756 is consistent with this source having a constant orbital period and a lower limit on the evolutionary timescale of

$$\tau_b = \frac{P_b}{|\dot{P}_b|} > 140\,\mathrm{Myr}. \qquad (8)$$

Binary evolution theory predicts that systems of this type evolve due to angular momentum loss through gravitational radiation (Kraft et al. 1962; Rappaport et al. 1982; Verbunt 1993). For conservative mass transfer, the binary period derivative is given by di Salvo et al. (2008),

$$\dot{P}_b = -4.4 \times 10^{-11}\frac{n - 1/3}{n + 5/3 - 2q}\left(\frac{P_b}{\mathrm{hr}}\right)^{-5/3}$$
$$\times \left(\frac{M_{NS}}{M_\odot}\right)\left(\frac{M_C}{M_\odot}\right)\left(\frac{M_{NS} + M_C}{M_\odot}\right)^{-1/3}\mathrm{s\,s^{-1}}, \qquad (9)$$

where M_{NS} is the neutron star mass, $q = M_C/M_{NS}$ is the binary mass ratio, and $-1/3 < n < 1$ is the mass–radius index of the companion star. Depending on the source inclination, Krimm et al. (2007b) derived a companion mass of $M_C = 0.007–0.022\,M_\odot$ for a neutron star mass of $1.4\,M_\odot$. For a neutron star mass of $2.2\,M_\odot$, the allowed range increased to $M_C = 0.009–0.030\,M_\odot$. In both cases, they assumed an upper limit on the inclination of $i < 85°$, motivated by the fact that Swift J1756 does not show eclipses in its light curve. Accounting for the extreme cases of stellar masses and n, the binary may either be contracting or expanding. In either case, however, the rate of change is limited to $|\dot{P}_b| \lesssim 7 \times 10^{-14}\,\mathrm{s\,s^{-1}}$, which is well below the upper limit obtained in this work.

Although the binary evolution timescale we obtain for Swift J1756 is consistent with theory, it is worth noting that this is not generally true for low-mass X-ray binaries (see Patruno et al. 2017, for a comprehensive discussion). The AMXP SAX J1808.4–3658, in particular, has been found to evolve on a much shorter timescale, with a first derivative on the orbital period of $3.5 \times 10^{-12}\,\mathrm{s\,s^{-1}}$ (Hartman et al. 2008; Patruno et al. 2012; Sanna et al. 2017a). Two models have been proposed to explain this discrepancy: highly nonconservative mass transfer due to irradiation of the companion star by the pulsar (di Salvo et al. 2008; Burderi et al. 2009), and spin–orbit coupling in the companion star (Hartman et al. 2008, 2009). While the latter depends on the companion star, and may vary from source to source, the former should operate in all AMXPs (see also Patruno 2017; Sanna et al. 2017c), including Swift J1756. The spin-down luminosity impinging on the companion star can be estimated as

$$\dot{E}_{abl} = -\frac{1}{4}\left(\frac{R_{L2}}{a}\right)^2\dot{E}_{sd}, \qquad (10)$$

where $\dot{E}_{abl}$ is the ablation luminosity, R_{L2} is the Roche lobe radius of the companion (Eggleton 1983), and a the binary separation. The irradiation fraction is $f = \dot{E}_{abl}/\dot{E}_{sd}$, which, accounting for the range of allowed neutron star and companion masses, evaluates to $f = 0.15\%–0.35\%$. The associated mass loss for the companion is given by

$$\dot{M}_C = -\eta\dot{E}_{abl}\frac{R_{L2}}{GM_C}, \qquad (11)$$

such that, assuming an efficiency of $\eta = 100\%$, $\dot{M}_C \sim -3 \times 10^{-10}\,M_\odot\,\mathrm{yr^{-1}}$. The effect of this mass loss on the orbital period follows through the relation (Frank

et al. 2002)

$$\frac{\dot{P}_b}{P_b} = -2\frac{\dot{M}_C}{M_C}, \tag{12}$$

giving a period derivative due to mass loss of $\dot{P}_{b,\mathrm{ML}} = 5 \times 10^{-12}$ s s^{-1}. This value is well above our limit on the period derivative. Hence, in order for this mechanism to be consistent with our observations of Swift J1756, the efficiency at which the companion star converts the incident luminosity into mass loss must be $\eta < 15\%$. This value is very different from the 40% required in SAX J1808.4–3658 (Patruno et al. 2016) and is instead in line with the $<5\%$ efficiency determined for IGR J00291+5934 (Patruno 2017).

ORCID iDs

Deepto Chakrabarty ⓘ https://orcid.org/0000-0001-8804-8946
Sebastien Guillot ⓘ https://orcid.org/0000-0002-6449-106X
Wynn C. G. Ho ⓘ https://orcid.org/0000-0002-6089-6836
Gaurava K. Jaisawal ⓘ https://orcid.org/0000-0002-6789-2723
Craig B. Markwardt ⓘ https://orcid.org/0000-0001-9803-3879
Paul. S. Ray ⓘ https://orcid.org/0000-0002-5297-5278
Tod E. Strohmayer ⓘ https://orcid.org/0000-0001-7681-5845

References

Bult, P., Patruno, A., & van der Klis, M. 2015, ApJ, 814, 138
Bult, P. M., Gendreau, K. C., Ray, P. S., et al. 2018a, ATel, 11502, 1
Bult, P. M., Gendreau, K. C., Ray, P. S., et al. 2018b, ATel, 11581, 1
Burderi, L., Di Salvo, T., Lavagetto, G., et al. 2007, ApJ, 657, 961
Burderi, L., Riggio, A., di Salvo, T., et al. 2009, A&A, 496, L17
di Salvo, T., Burderi, L., Riggio, A., Papitto, A., & Menna, M. T. 2008, MNRAS, 389, 1851
Eggleton, P. P. 1983, ApJ, 268, 368
Frank, J., King, A., & Raine, D. J. 2002, Accretion Power in Astrophysics: Third Edition (Cambridge: Cambridge Univ. Press)
Gendreau, K., & Arzoumanian, Z. 2017, NatAs, 1, 895
Gendreau, K. C., Arzoumanian, Z., Adkins, P. W., et al. 2016, Proc. SPIE, 9905, 99051H
Gierliński, M., Done, C., & Barret, D. 2002, MNRAS, 331, 141
Hartman, J. M., Patruno, A., Chakrabarty, D., et al. 2008, ApJ, 675, 1468
Hartman, J. M., Patruno, A., Chakrabarty, D., et al. 2009, ApJ, 702, 1673
Hobbs, G. B., Edwards, R. T., & Manchester, R. N. 2006, MNRAS, 369, 655
Ibragimov, A., & Poutanen, J. 2009, MNRAS, 400, 492
Jahoda, K., Markwardt, C. B., Radeva, Y., et al. 2006, ApJS, 163, 401
Kraft, R. P., Mathews, J., & Greenstein, J. L. 1962, ApJ, 136, 312
Krimm, H. A., Barthelmy, S. D., Barbier, L., et al. 2007a, ATel, 1105, 1
Krimm, H. A., Markwardt, C. B., Deloye, C. J., et al. 2007b, ApJL, 668, L147
Manchester, R. N., & Peters, W. L. 1972, ApJ, 173, 221
Markwardt, C. B., Krimm, H. A., & Swank, J. H. 2007, ATel, 1108, 1
Mereminskiy, I. A., Grebenev, S. A., Krivonos, R. A., & Sunyaev, R. A. 2018, ATel, 11497, 1
Mukherjee, D., Bult, P., van der Klis, M., & Bhattacharya, D. 2015, MNRAS, 452, 3994
Patruno, A. 2010, ApJ, 722, 909
Patruno, A. 2017, ApJ, 839, 51
Patruno, A., Altamirano, D., & Messenger, C. 2010, MNRAS, 403, 1426
Patruno, A., Bult, P., Gopakumar, A., et al. 2012, ApJL, 746, L27
Patruno, A., Jaodand, A., Kuiper, L., et al. 2017, ApJ, 841, 98
Patruno, A., Maitra, D., Curran, P. A., et al. 2016, ApJ, 817, 100
Patruno, A., Markwardt, C. B., Strohmayer, T. E., et al. 2009, ATel, 2130, 1
Patruno, A., & Watts, A. L. 2012, arXiv:1206.2727
Prigozhin, G., Gendreau, K., Foster, R., et al. 2012, Proc. SPIE, 8453, 845318
Rappaport, S., Joss, P. C., & Webbink, R. F. 1982, ApJ, 254, 616
Riggio, A., Papitto, A., Burderi, L., et al. 2011, A&A, 526, A95
Sanna, A., Bahramian, A., Bozzo, E., et al. 2018, A&A, 610, L2
Sanna, A., Di Salvo, T., Burderi, L., et al. 2017a, MNRAS, 471, 463
Sanna, A., Papitto, A., Burderi, L., et al. 2017b, A&A, 598, A34
Sanna, A., Pintore, F., Bozzo, E., et al. 2017c, MNRAS, 466, 2910
Shapiro, I. I., Ash, M. E., Ingalls, R. P., et al. 1971, PhRvL, 26, 1132
Spitkovsky, A. 2006, ApJL, 648, L51
Strohmayer, T., & Keek, L. 2017, ApJL, 836, L23
Verbunt, F. 1993, ARA&A, 31, 93
Wijnands, R., & van der Klis, M. 1998, Natur, 394, 344